



**HAL**  
open science

## Comparison between SANS and APT measurements in a thermally aged Fe-19 at.%Cr alloy

O. Tissot, Cristelle Pareige, M.-H. Mathon, Manuel Roussel, E. Meslin, B.  
Décamps, J. Henry

► **To cite this version:**

O. Tissot, Cristelle Pareige, M.-H. Mathon, Manuel Roussel, E. Meslin, et al.. Comparison between SANS and APT measurements in a thermally aged Fe-19 at.%Cr alloy. *Materials Characterization*, 2019, 151, pp.332-341. 10.1016/j.matchar.2019.03.027 . hal-02106979

**HAL Id: hal-02106979**

**<https://normandie-univ.hal.science/hal-02106979>**

Submitted on 29 May 2019

**HAL** is a multi-disciplinary open access archive for the deposit and dissemination of scientific research documents, whether they are published or not. The documents may come from teaching and research institutions in France or abroad, or from public or private research centers.

L'archive ouverte pluridisciplinaire **HAL**, est destinée au dépôt et à la diffusion de documents scientifiques de niveau recherche, publiés ou non, émanant des établissements d'enseignement et de recherche français ou étrangers, des laboratoires publics ou privés.

## Comparison between SANS and APT measurements in a thermally aged Fe-19 at.%Cr alloy

O. Tissot<sup>a,\*</sup>, C. Pareige<sup>b</sup>, M.-H. Mathon<sup>c</sup>, M. Roussel<sup>b</sup>, E. Meslin<sup>c</sup>, B. Décamps<sup>d</sup>, J. Henry<sup>a</sup>

<sup>a</sup> DEN-Service de Recherches Métallurgiques Appliquées, CEA, Université Paris-Saclay, F-91191 Gif-sur-Yvette, France

<sup>b</sup> Normandie Univ, UNIROUEN, INSA Rouen, CNRS, Groupe de Physique des Matériaux, 76000 Rouen, France

<sup>c</sup> DEN-Service de Recherches de Métallurgie Physique, CEA, Université Paris-Saclay, F-91191 Gif-sur-Yvette, France

<sup>d</sup> Centre de Sciences Nucléaires et de Sciences de la Matière (CSNSM), CNRS/IN2P3, Univ. Paris-Sud, Bât. 108, Université Paris-Saclay, 91405 Orsay, France

<sup>e</sup> Laboratoire Léon Brillouin, CEA-CNRS, Université Paris-Saclay, F-91191 Gif-sur-Yvette, France

### ABSTRACT

$\alpha'$  precipitation in a Fe-19 at.%Cr alloy aged at 500 °C up to 2008 h has been characterized by both APT and SANS. This paper shows that when using an appropriate method for SANS data treatment, both APT and SANS yield consistent results regarding not only volume fraction and size but also  $\alpha$  and  $\alpha'$  composition. Good agreement is achieved when  $\alpha'$  particles are considered as magnetic scattering features at the early stage of the kinetics.

### 1. Introduction

High chromium Ferritic/Martensitic (F/M) steels and Oxide Dispersion Strengthened (ODS) alloys are considered for nuclear application owing to their excellent swelling resistance, small ductile-to-brittle transition temperature (DBTT) shift and good thermal properties [1–5]. FeCr alloys are the base of these F/M and ODS alloys. Thus, a thorough understanding of the mechanisms involved during thermal ageing or irradiation of FeCr alloys is a key issue. In particular, the characterization of the  $\alpha'$  precipitation, well known for embrittling alloys, has been carried out after thermal ageing [6,7] and after several irradiation conditions [8–13]. Small Angle Neutron Scattering (SANS) as well as Atom Probe Tomography (APT) are frequently used to study  $\alpha$  -  $\alpha'$  decomposition as they are well suited for characterizing nanoscale precipitates. Both techniques give information about size, volume fraction and composition of phases. Nevertheless, each technique has its own weaknesses and strengths. To provide composition of phases and particle size, the treatment of SANS data relies on models and assumptions about the investigated microstructure. If different scatters of similar size are present in the sample, their detection and discrimination are not possible. On the other hand, the probed volume in a typical SANS experiment is of the order of 10 to 100 nm<sup>3</sup> making SANS experiments statistically reliable. APT gives access to 3D reconstruction of the investigated volume and chemical composition measurements at the atomic scale. APT is sensitive to dilute and small objects and the different families of nano-features can be discriminated. However, the

small size of the probed volume (typically 80 × 80 × 250 nm<sup>3</sup>) limits APT ability to detect objects with a low density ( $D_v > 6.25 \cdot 10^{20} \text{ m}^{-3}$  in this case). Moreover, APT relying on physics of field evaporation of atoms, artefacts may appear that can artificially modify shape and composition of the observed particles [14–19]. Respective weaknesses and strengths of SANS and APT make them complementary techniques and cross-checking results obtained for the same alloys is of a large interest [20–22]. Nevertheless, one very important point is still pending. It concerns the composition of the particles. Indeed, while studies on  $\alpha'$  precipitation carried out by both SANS and APT agree reasonably well on the radius and/or volume fraction and  $\alpha$  equilibrium composition, a large discrepancy regarding  $\alpha'$  composition is always observed at early stage. The APT study of Novy et al. [7] performed on a Fe-20 at.%Cr alloy thermally aged at 500 °C, has shown evolution of  $\alpha'$  precipitates composition with ageing time, whereas Bley et al. [6] assumed that  $\alpha'$  precipitation took place with the equilibrium composition. A similar disagreement has been found on precipitates formed in Fe-12 at.%Cr irradiated at 300 °C with neutrons. Kuksenko et al. [9] measured an  $\alpha'$  precipitate composition different from equilibrium with APT whereas Bergner et al. [8] made the assumption, in their SANS data treatment approach, that  $\alpha'$  particles have the equilibrium composition. Bergner et al. [10] addressed this issue of discrepancy between APT and SANS results by performing SANS data treatments based on APT results and taking into account a set of potential sources of deviation. However that was not sufficient for removing the discrepancy on  $\alpha'$  particles' composition. Prior work of Hyde et al. [20] on radiation

\* Corresponding author.

E-mail address: [olivier.tissot@cea.fr](mailto:olivier.tissot@cea.fr) (O. Tissot).

induced clusters in Reactor Pressure Vessel (RPV) steels using APT and SANS lead to similar conclusions. Recently, Couturier et al. [23] developed a common framework for comparing SAXS (Small Angle X-ray Scattering) with APT results when applied to spinodal decomposition in Fe-Cr steels. Contrary to prior studies, agreement was found on the amplitude of composition fluctuations but not on the wavelength of the interconnected structure; thus discrepancy still remains. In fact, the discrepancy between SANS and APT results exists since many years and has been noted in studies performed on a wide variety of alloys [24–26].

Except in the case of Couturier et al. [23], the main issue between APT and SANS concerns the composition of precipitates. As stressed by Hyde et al. [20], solution of this issue is hidden behind the limitations of the two techniques and assumptions used for data treatment. One of the most obvious explanation could be the so called local magnification effect [14,27] observed in APT experiments when two phases present different evaporation fields. This artefact originates from the fact that  $\alpha'$  particles' evaporation field is lower than the matrix one. It leads to a focussing of the ion trajectories. This focussing may imply two different behaviours depending on the evaporation field difference of the phases [18,19]: 1) a simple compression of the precipitates in the x-y plane of the analysis volume without incorporation of matrix elements into the precipitates, only modification of the shape is observed, particles appear with an ellipsoidal shape, 2) compression and incorporation of matrix atoms inside the precipitates that can lead to an artificial dilution of low field precipitates. In both case, the shape is ellipsoidal and an increase in atomic density is observed: in case 1, the number of atoms coming from the particles being constant but the volume of the precipitate after reconstruction being smaller because of the compression, the atomic density is increased. In case (2), in addition to the increase described in case (1), addition of atoms coming from the surrounding matrix is also observed [18,19]. So, it is worth noting that increase in atomic density does not systematically imply mixing of matrix and particle atoms. Depending on the difference in evaporation field between precipitates and matrix, trajectory overlaps at the interface between matrix and precipitates are more or less important. For case 1 (when field evaporation difference is low) only interfaces between precipitates and matrix are affected. Therefore, the core composition of precipitates remains correct. In case 2, when the difference in evaporation field is too big, incorporation of matrix elements in precipitates is no more negligible and can affect the core composition of the precipitates. If trajectory overlaps are important and affect more than the interfaces, small clusters will be more affected than larger ones. In the Fe-Cr case, the Cr bulk evaporation field is  $29 \text{ V}\cdot\text{nm}^{-1}$  whereas the Fe bulk evaporation field is  $33 \text{ V}\cdot\text{nm}^{-1}$  [28]. As the Cr concentration of precipitates goes up, the evaporation field of precipitates decreases and the local magnification effect is more pronounced.

The question is: do  $\alpha'$  particles belong to case 1 (compression of clusters without incorporation of matrix atoms in the precipitates, only interfaces are affected) or to case 2 (incorporation of matrix atoms up to the core of the precipitates with artificial dilution of precipitates)? The authors showed in previous works using both simulation of field evaporation of  $\alpha'$  particles and experimental data [7,29] that the core composition of  $\alpha'$  particles appears to be unaffected and that local magnification effect in Fe-Cr belongs to case 1.

Another possible explanation of the discrepancy between SANS and APT results is that classical assumptions on which SANS data treatment relies are not appropriate for this system. Hyde et al. [20] showed that, depending on the assumptions made very different results can be obtained using SANS. It must be pointed out that only reasonable assumptions were considered. From their study they concluded that SANS A-ratio cannot be used to conclude on the Fe concentration in clusters. Their study also revealed the strong impact of the assumption regarding the magnetic properties of clusters on the results. In reported work [see for example [6,8]],  $\alpha'$  particles are thought to be non-magnetic

scattering features. But if, as suggested by APT measurements,  $\alpha'$  precipitates contain a Fe concentration higher than 30% at short ageing time, this assumption no longer holds and  $\alpha'$  particles have to be treated as magnetic scattering features.

Based on an experimental study by SANS and APT of  $\alpha - \alpha'$  decomposition in a Fe-19 at.%Cr thermally aged at  $500^\circ\text{C}$ , the objective of the present paper is to demonstrate that both techniques can agree on all the characteristics of  $\alpha'$  precipitates including the composition, providing  $\alpha'$  particles are considered to be magnetic scattering features.

Section 2 of this paper is devoted to experimental details. Results and discussion on the kinetics of  $\alpha'$  precipitation, studied by Atom Probe Tomography and SANS, are presented in Section 3.

## 2. Materials and methods

### 2.1. Materials

The studied material is a high purity Fe-19 at.%Cr alloy that was prepared by induction melting at Ecole des Mines de Saint Etienne in France. Composition was determined using Glow Discharge Mass Spectrometry. The alloy was received in a recrystallized state, after 70% cold reduction and 1 h -  $850^\circ\text{C}$  heat treatment under pure argon that was followed by air-cooling to room temperature. The resulting mean grain size and dislocation density were  $650 \mu\text{m}$  and  $< 10^{12} \text{ m}^{-2}$  respectively. The thermal ageing has been carried out in a muffle furnace at  $500^\circ\text{C}$ . The temperature of the furnace was controlled by a thermocouple located in the middle of the heating zone. A second thermocouple, in contact with the samples, has been used to obtain a more accurate value of the temperature (here  $510^\circ\text{C}$ ). Samples of  $15 \times 10 \text{ mm}$  and 1 mm thick were encapsulated in quartz cells under high vacuum ( $5 \times 10^{-6} \text{ mbar}$ ) with zirconium chips to prevent oxidation. Thermal ageing has been realized during 50 h, 100 h, 240 h, 480 h, 986 h and 2008 h.

### 2.2. Methods

#### 2.2.1. Atom Probe Tomography

The APT samples were prepared from  $0.3 \times 0.3 \times 15 \text{ mm}$  stick. They were obtained by choosing suitable electro polishing conditions (75% acetic acid – 25% perchloric acid, 7 to 5 V and 98% ether – 2% perchloric acid 7 to 4 V). The samples were analysed using two different LEAP 4000X HR Atom Probes from CAMECA having a high mass resolution  $((M/\Delta M)_{1\%} = 233$  for the major peak of Fe) and a detector efficiency of 36 or 42% depending on the LEAP used. The samples were cooled down to a temperature of 55 K in order to mitigate the preferential field evaporation of Cr atoms. During analyses, the atom probe specimens were electrically pulsed with a pulse fraction of 20%, a pulse rate of 200 kHz and a detection rate of 0.003 atom per pulse. Reconstructions of the volumes were done with IVAS 3.6.8 (CAMECA software) using the same parameters as in [12]: a compression factor of 1.4–1.5, an evaporation field of  $33 \text{ V}\cdot\text{nm}^{-1}$  and a k factor of 3.25–4.5.

Data treatments were performed thanks to the 3D Data Software for Atom Probe Tomography developed by the GPM research group in Rouen, France. Measurement of the size and number density of clusters was performed using the “isoposition” concentration data filter [17,30,31]. The filter enables to distinguish the particles from the surrounding matrix owing to their chemical composition. The parameters used were: concentration threshold  $X_{\text{Cr}} > 28 \text{ at.}\%$ , grid pattern of 1 nm, separation distance  $d = 0.2 \text{ nm}$  and a minimum number of atoms in the particles of 95. This method is shown to be the most efficient to discriminate clusters from the surrounding matrix [17]. The cluster composition was measured using erosion profile [16]. The core corresponds to the plateau appearing on the profiles. The number density of the particles was determined by a simple ratio of the number of observed precipitates to the overall analysed volume. The radius of each precipitate was deduced from the number of Cr and Fe atoms in

each particle considering spherical particles:  $R = \sqrt[3]{\frac{3nV_{at}}{4\pi Q}}$  with  $V_{at}$  the Fe atomic volume and  $Q$  the detector efficiency. This calculation is valid as far as no atoms coming from the surrounding matrix are incorporated in the precipitates. The volume fraction was defined as the ratio of the number of atoms inside the precipitates to the total number of collected atoms. Agreement with volume fraction values deduced from phase composition using lever rule has been checked in each case. The basic principle of APT and data treatment may be found in different books or reviews [16,32–35].

## 2.2.2. Small Angle Neutron Scattering

### • Technical aspects

The neutron scattering experiments were performed at the Laboratoire Léon Brillouin (CEA CNRS), Saclay, on PAXY small-angle instrument which have 2-dimensional detector allowing anisotropic scattering intensity acquisition. The study of precipitate sizes ranging between 0.5 nm and about 20–30 nm needs two different configurations of measurement which are defined by the wavelength ( $\lambda$ ) and the sample-to-detector distance. The wavelength can be chosen between 0.55 nm because of multiple diffraction effect due to the iron matrix, and about 1 nm because, above multiple scattering can occur. As a consequence, the best configurations for steels characterization available at LLB, are 0.6 nm/2 m and 0.9 nm/5 m covering a scattering vector ( $q$ ) range from 0.08 to  $1.6 \text{ nm}^{-1}$  ( $q = 4\pi\sin\theta/\lambda$  where  $2\theta$  is the scattering angle). The magnetic interaction between the magnetic moment of the neutron and the atoms of the material is anisotropic: the scattering length depends only on the magnetic moment component perpendicular to  $\vec{q}$ . In the case of ferromagnetic materials, the magnetic moment can be aligned along an applied saturating magnetic field. The magnetic contribution should be zero in the field direction and maximum in the perpendicular direction. Consequently, nuclear plus magnetic and nuclear contributions can be separated. Angular sectors of 20% around the two directions (parallel and perpendicular to the applied magnetic field) were considered for calculations. The value of the applied magnetic field required to reach the saturation of the magnetization varies with the alloy composition, internal stresses, etc. Here, the measurements were performed under a saturating field of 1.5 T. Two sample dimensions have been characterized depending on the available quantity of materials (sample dimension were either 10 mm  $\times$  10 mm of surface and 1 mm of thickness or 7 mm  $\times$  4 mm of surface and 1 mm of thickness). The final results do not depend on the sample shape. Initial data treatment including correction, normalization, and calibration, has been described by Cotton [36].

### • The analysis method

In the case of ferromagnetic materials, the SANS intensity is the sum of two contributions, a nuclear and a magnetic, which depend respectively on the difference in composition and in magnetization between particles and the matrix. In terms of cross-section, the SANS intensity can be written as:

$$\left(\frac{d\Sigma}{d\Omega}\right)(q) \approx f_p [\Delta\rho_{nucl}^2 + \Delta\rho_{mag}^2 \sin^2 \delta] F^2(q, R, h(R)) S(q, R)$$

where  $q$  is the scattering vector,  $f_p$  the precipitate atomic fraction, and  $F(q, R)$  is the form factor of the particles, which can include a size distribution function  $h(R)$ .  $S(q, R)$  is the interference term, which is negligible for precipitate fractions lower than 1% ( $S(q, R) = 1$ ). For volume fractions higher than  $\approx 1\%$ , the Wertheim [37] and Thiele [38] analytical solution of the total correlation function  $u(r)$  is used:

$$u(r) = -(\alpha + \beta s + \gamma s^3) \quad \text{with} \quad s = r/2R, \quad \alpha = (1 + 2\eta)^2/(1 - \eta)^4, \\ \beta = -6\eta(1 + \eta/2)^2/(1 - \eta)^4 \quad \text{and} \quad \gamma = \eta\alpha/2. \quad \eta \text{ is the volume fraction of hard spheres, } R \text{ is the radius of hard spheres and } r \text{ the radius of}$$

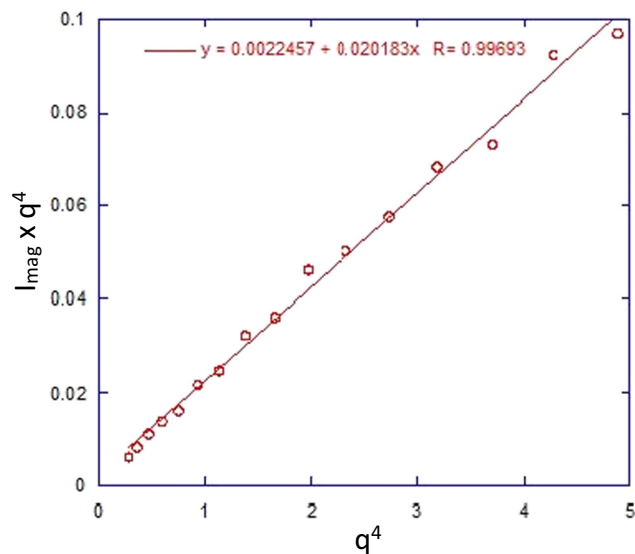


Fig. 1. Scattered intensity multiplied by  $q^4$  as a function of  $q^4$  for a Fe-19 at.%Cr reference sample (not aged).

particles. The hard sphere represents an area around a precipitate in which no other precipitate could appear. The hard sphere existence is justified by the local depletion of Cr in matrix due to the nearby precipitate which do not allow another precipitation in this zone. It also represents a non-interpenetration zone.

$$S(\mathbf{q}) = \frac{1}{1 - NC(\mathbf{q}, R, \eta)} \quad \text{with} \quad C(\mathbf{q}, R, \eta) \\ = -4\pi(2R)^3 \int_0^1 (\alpha + \beta s + \gamma s^3) \frac{\sin(sq2R)}{sq2R} s^2 ds.$$

$\Delta_{nucl \text{ or } mag}$  are the nuclear or magnetic contrasts given by:

$$\Delta_{nucl \text{ or } mag} = \frac{b_{nucl \text{ or } mag}^p}{v_{at}^p} - \frac{b_{nucl \text{ or } mag}^m}{v_{at}^m}$$

where  $b$  is the nuclear (nucl) or magnetic (mag) mean scattering length in the precipitates (p) or in the matrix (m), and  $v_{at}^p, v_{at}^m$  is the mean atomic volume of the precipitates (p) and of the matrix (m).  $\delta$  is the angle between the magnetization of the sample and the scattering vector  $q$ . As the experiment was performed under magnetic field, the atomic magnetic moments were aligned along the applied magnetic field. So the angle  $\delta$  is known and the scattered intensities obtained in the two  $\perp$  and  $\parallel$  to H directions corresponding to  $\delta = 90^\circ$  and  $\delta = 0^\circ$  respectively can be considered separately. Assuming that the form factors corresponding to the nuclear and magnetic scattering are the same which is true for homogeneous particles, the difference of these two contributions gives the magnetic scattering:

$$\left(\frac{d\Sigma}{d\Omega}\right)(q) \approx f_p \Delta\rho_{mag}^2 F^2(q, R, h(R))$$

The ratio between these two contributions is called ‘‘A ratio’’. For homogeneous particles with sharp interfaces, it depends only on the chemical composition, magnetization and atomic density variations between precipitates and the matrix, and is given by:

$$A = \frac{\left(\frac{d\Sigma}{d\Omega}\right)_{\perp H}}{\left(\frac{d\Sigma}{d\Omega}\right)_{\parallel H}} = 1 + \frac{\Delta\rho_{mag}^2}{\Delta\rho_{nucl}^2}$$

This ratio can provide information about the chemical composition of the particles.

The magnetic scattering length is defined by  $b_{mag, matrix} = -\gamma r_0/2\mu$ , where  $\gamma = -1.913$  is the gyromagnetic factor of the neutron,

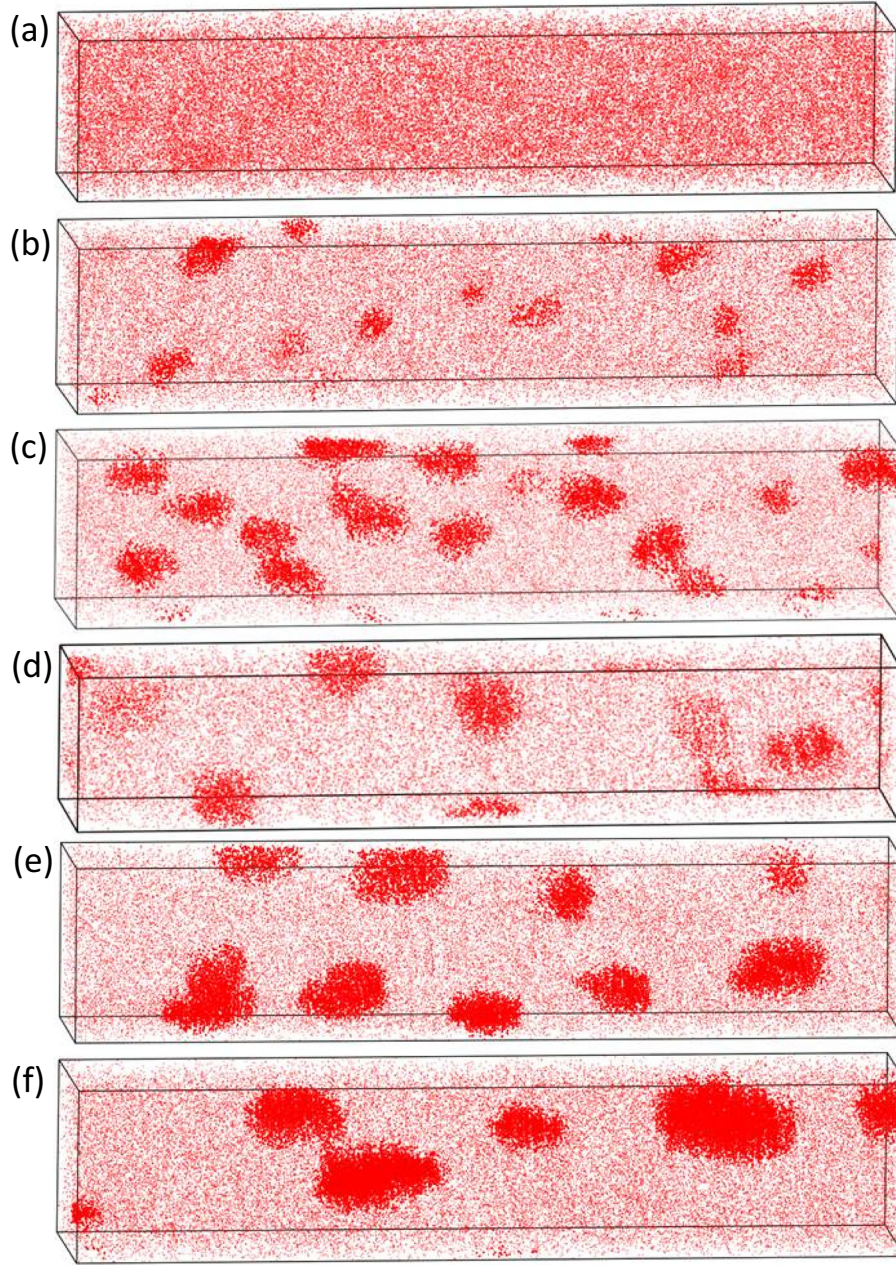


**Fig. 2.** 3D atom maps of Cr atoms in a Fe-19 at.%Cr alloy aged (a) 50 h, (b) 100 h, (c) 240 h, (d) 480 h, (e) 976 h and (f) 2008 h. A concentration threshold of  $X_{Cr} > 28$  at.% was used to highlight  $\alpha'$  precipitate ( $V = 10 \times 10 \times 50$  nm<sup>3</sup>).

$r_0 = 0.2818 \times 10^{-14}$  m is the classical electron radius and  $\mu$  is the mean magnetic moment of atoms. Only iron atoms present a magnetic moment which is slightly different from that of pure iron. An estimation of the average magnetic moment of the system, assuming that the mean effect is due to the Cr atomic concentration  $C_{Cr}$ , is obtained with the relation  $\mu = \mu_{Fe} - 2.39 C_{Cr}$  in Bohr magneton units [39],  $\mu_{Fe}$  is equals to 2.217.

Above 70% chromium in the particles, the average magnetic moment of iron atoms in the Fe-Cr system is zero at room temperature [40]. As a first method of data treatment, Cr rich precipitates ( $\alpha'$ ) will be considered to have the equilibrium composition ( $\approx 86$  at.%Cr). This corresponds to the most used method in the literature to treat SANS data [6,8,41]. In such case, the magnetic scattering length  $b_{mag, \alpha'}$  will be zero. We will see that under this assumption, agreement is not achieved for all the characteristics of  $\alpha/\alpha'$  phase separation. Thus, we will present a second method based on the use of  $\alpha$  and  $\alpha'$  compositions

measured with APT to fit SANS data. As will be explained in the following,  $\alpha'$  precipitates will be treated as ferromagnetic particles when Cr content is below 70%.

At high angle, SANS intensity tends towards a minimal value which is the background noise. If the asymptotic Porod's [42] behaviour is reached, a linear variation at high angle of  $I_{mag} \times q^4 = f(q^4)$  should be observed and the slope would represent the background noise. It is indeed observed in our case, for the reference sample which presents no precipitation as shown in Fig. 1. As part of data treatment the background noise was subtracted for the experimentally measured diffused intensities of the aged samples.

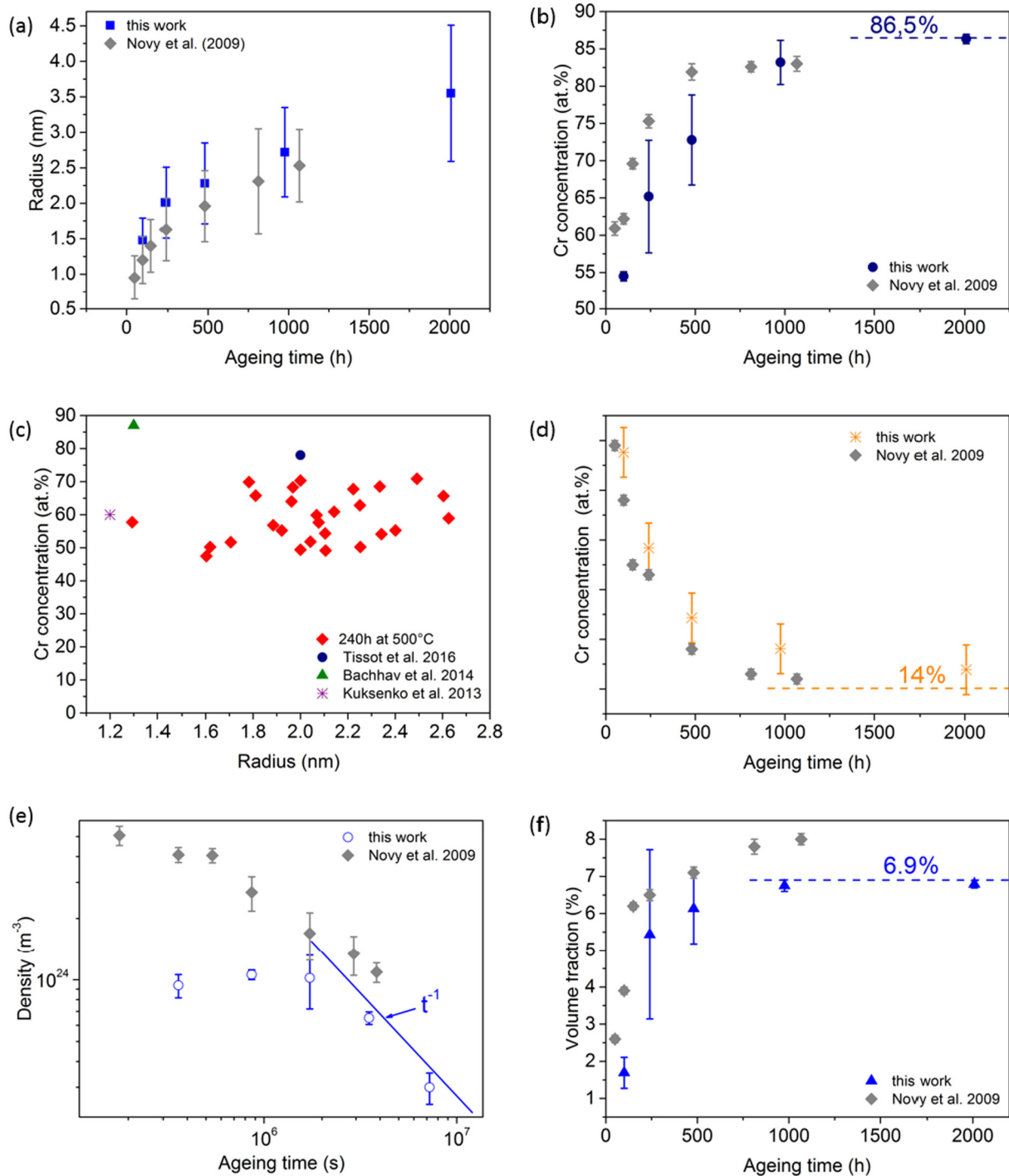


**Fig. 3.** (a) Mean radius evolution of  $\alpha'$  particles as a function of ageing time (b) evolution of Cr composition of the  $\alpha'$  particles as a function of ageing time. The errors represent the spread of the measures, (c) core Cr concentration of  $\alpha'$  precipitates as a function of their mean radius in after ageing 240 h and from literature, (d) Cr concentration of the matrix as a function of ageing time. The horizontal line represents the solubility limit determined by Novy et al. [7] and Dubiel et al. [44], (e) particles density as a function of ageing time. The straight line represents the  $t^{-1}$  law (predicted for long ageing time), (f) evolution of volume fraction of  $\alpha'$  phase in function of ageing time. The dashed line represents the equilibrium value deduced from the Lever Rule with compositions given by the phase diagram of Xiong et al. [40]. The errors bars show the dispersity of the measures; in a Fe-19 at.%Cr aged at 500 °C. Grey diamond represent the data of Novy et al. [7] for a Fe-20 at.%Cr.

### 3. Results and discussion

#### 3.1. Atom Probe Tomography characterization

First, the as-received state was characterized to check the Cr distribution. Cr atoms distribution has been compared to the binomial distribution, which corresponds to random distribution of atoms using

the Thuvander et al. method [43]. Results show that Cr distribution is random in the as-received state.

The 3D atom maps of Cr atoms following ageing at 500 °C during 50 h, 100 h, 240 h, 480 h, 976 h and 2008 h are presented in Fig. 2. After 50 h ageing, whereas no Cr precipitates were clearly distinguished in the APT volumes, the Thuvander et al. test [43] showed that phase separation already started for this ageing time. As soon as 240 h of

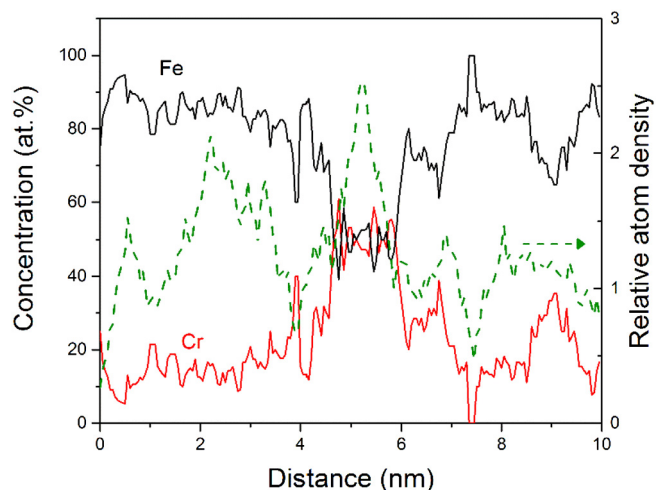


Fig. 4. Linear concentration profile drawn through a 1 nm radius precipitate in the x-y plan in the Fe-15%atCr alloy aged 240 h at 500 °C. Also reported, the relative atom density (number of atoms in the sampling volume over the mean number of atom in the matrix). A plateau at 57 at.%Cr is clearly visible. No correlation between Cr concentration and variation of the relative atom density.

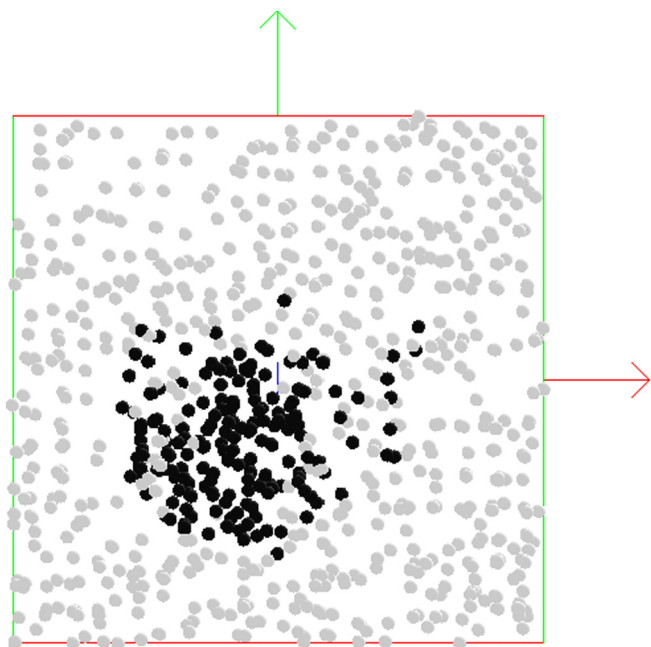


Fig. 5. X-Y atom map ( $V = 3 \times 3 \times 0.5 \text{ nm}^3$ ) of a Cr rich precipitate as obtained after simulation of field evaporation of a 1 nm radius precipitate containing 80 at.%Cr embedded in a Fe-14 at.%Cr matrix. Black atoms are Fe and Cr atoms from the precipitate. Grey atoms are Fe and Cr atoms of the matrix. This atom map corresponds to the concentration profile and the atom density profile published in [29].

annealing, some precipitates have an ellipsoidal shape whose major axis is along the analysis direction (Fig. 3(b-f)). This is the result of the focusing of ions as explained in the introduction [14,27].

Evolution of the mean radii of clusters, Cr concentration in particles and in the matrix, volume fraction and number density are given in Fig. 3 together with the data obtained by Novy et al. [7] in a Fe-20 at.%Cr aged at the same temperature. Results are in very good agreement. The small shift observed between the two data sets is due to the difference in driving force because of the difference in nominal composition (19 at.% versus 20 at.%).

As shown in Fig. 3(b), the composition of  $\alpha'$  precipitates evolves

with ageing time, ranging from  $(54.5 \pm 0.6) \text{ at.}\% \text{Cr}$  after 100 h ageing to  $(86.3 \pm 0.6) \text{ at.}\% \text{Cr}$  at 2008 h. The question is: does the small Cr concentration of the precipitates observed after 100 h and 240 h are due to artificial mixing with matrix atoms (case 2) or is it kinetics (case 1)? In order to answer this question the evolution of Cr concentration of precipitates as a function of their radius as measured after 240 h ageing is reported in Fig. 3(c) together with measurements done by Tissot et al. in a Fe-15%Cr alloys irradiated with electrons [12], Bachhav et al. in a Fe-15Cr alloy neutron irradiated up to 1.82 dpa dPa at 290 °C [11], Kuksenko et al. in Fe-12Cr and Fe9Cr neutron irradiated at 300 °C up to 0.6 dpa [9]. There is clearly no correlation between the size and the concentration of particles. Rather, Cr content depends on the ageing conditions. For example, considering a radius of 1.2–1.3 nm, Cr content ranges from 55% (short ageing time at 500 °C or low irradiation dose at 300 °C) to 87% (high irradiation dose at 300 °C). Moreover, particles presenting the highest Cr content are among the smallest one [11].

Conversely to what is shown here, Chen et al. [45] observed that core Cr concentration increases with cluster size in Fe-Cr alloys neutron irradiated at 300 °C and 450 °C. They also noticed that no concentration plateau in Cr was observed in the core of the precipitates. It must be emphasized that it is not the case in this work and in previous works where plateaus were observed [7,29]. It is worth noting that increase in Cr concentration with size is difficult to interpret [13] as it is difficult to separate artefact from kinetics effects. Indeed, interphase surface energy is one of the main factor determining the Cr content of the clusters in Fe-Cr [46] and the composition of the clusters can differ from equilibrium composition of the  $\alpha'$  phase [47,48]. Fig. 4 presents a concentration profile drawn through a precipitate 1 nm in radius. A plateau at 57 at.% Cr is clearly visible. The relative atom density (number of atoms in the sampling box over the mean number of atoms in the matrix) is also reported evidencing an increase in atomic density due the local magnification effect. Fig. 5 presents an XY atom map obtained by simulation of field evaporation, model developed by Vurpillot et al. [27], of a precipitate of 1 nm in radius. The simulation of field evaporation was performed on an Fe-Cr tip containing 1 nm radius precipitates 80 at.%Cr surrounded by an Fe matrix with a Cr concentration of 14 at.%. Black atoms are Cr atoms from the precipitate, grey atoms are atoms coming from the matrix. This atom map corresponds to the concentration profile and the atom density profile published in [29]. According to these simulations, the core of the precipitate is not affected by matrix atoms. Moreover, the experimental relative atom density profile (Fig. 4) is identical to the simulated relative atom density profile published in [29] which corresponds to the atom map in Fig. 5. This shows that simulations reproduce very well the experimental behaviour. Accordingly with the atom map, the linear concentration profile drawn through the simulated particle in [29] shows that the atom density peak is not due to atoms coming from the surrounding matrix but rather is mainly due to the contraction of the particle in XY plane without mixing. Consequently, it appears reasonable to not consider the excess of atom density as an overlap with matrix atoms.

### 3.2. Small Angle Neutron Scattering measurements – comparison with APT

Two data treatments were carried out for SANS experiments. First, the most used method in the literature to treat SANS data was performed i.e. composition of  $\alpha'$  precipitates was considered as constant with ageing time and equal to the attempted equilibrium composition (86%Cr-14%Fe) i.e.  $\alpha'$  particles were non-magnetic.

- First method of SANS data treatments

Fig. 6 shows the scattering spectrum (a) perpendicular and (b) parallel to the magnetic field,  $H$  ( $H = 1.5 \text{ T}$ ) of the Fe-19 at.%Cr alloy before ageing and aged between 50 h and 2008 h. In good agreement with APT results, no scattering was observed for  $q > 0.03 \text{ nm}^{-1}$  in the

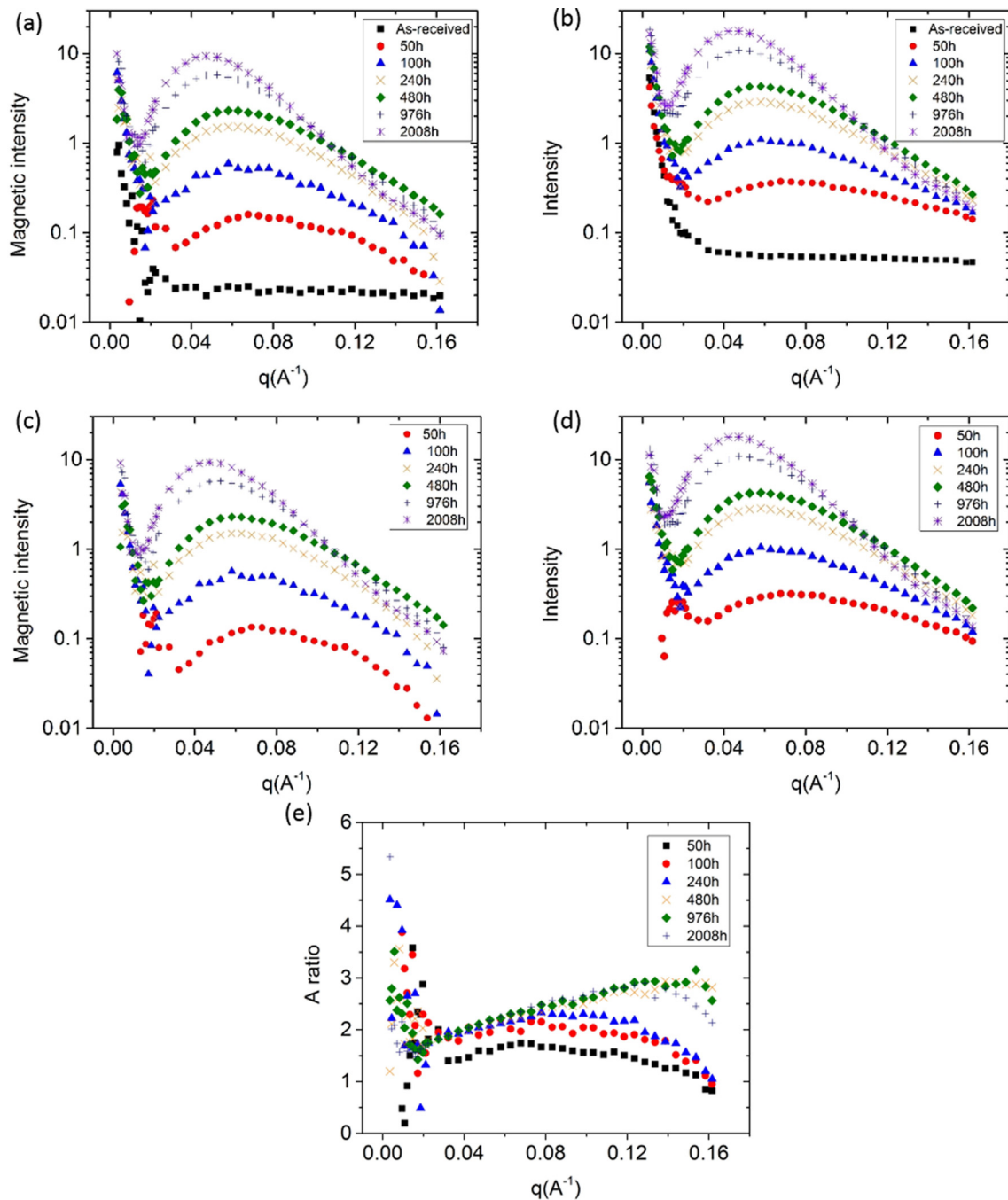


**Fig. 6.** Scattering intensity and A ratio spectrum in function of the scattering vector  $q$ , obtained in Small Angle Neutron Scattering measurements of a Fe-19 at.%Cr alloy aged between 50 h and 2008 h, (a) magnetic intensity (b) nuclear intensity perpendicular to the horizontal magnetic field (c) magnetic difference scattering cross-section (as-received subtracted from (a)) (d) nuclear difference scattering perpendicular to the horizontal magnetic field (e) A ratio (as-received subtracted).

as-received state; the intensity scattered at very small  $q$  is due to the microstructure (grains, grain boundaries etc.) and is not affected by the thermal treatments. In the initial state, Cr repartition was homogenous. Regarding the aged alloys, scattering peaks were clearly seen even after 50 h annealing. The position of the peak maximum is related to the distance between precipitates. Fig. 6(a) to (d) shows that with the annealing time, the scattered intensity increases because of the growth of the size and/or the volume fraction precipitated and the peak shifts towards the small  $q$  which is consistent with the increase in distance between particles. Thanks to the perpendicular and parallel intensity measurements, the A ratio was determined. The deduced A ratio increases with the ageing time: values of  $1.6 \pm 0.1$ ,  $2.0 \pm 0.1$  and  $2.25 \pm 0.1$  are obtained after 50 h, 100 h and above 480 h

respectively. The calculation of theoretical values of A needs some assumptions concerning the chemical composition in Fe and Cr, the average magnetic moment and the atomic density in matrix and precipitates. A value of 1.6 can correspond to 80%Cr-Fe20% particles in a super-saturated matrix Fe81%-Cr19%. An A ratio value of 2.2 can be attributed either to non-magnetic Cr-rich  $\alpha'$  particles (90% Cr-10% Fe) [8,41] or  $\alpha'$  particles richer in iron and ferromagnetic (30% Fe-70% Cr) in a Fe88% -Cr12% and Fe85% -Cr15% matrix respectively. In fact, conclusion on  $\alpha'$  composition is difficult to get. The SANS results in terms of the A-ratio demonstrate that the compositions of both the matrix and the particles evolve towards the equilibrium compositions.

Size and volume fraction of  $\alpha'$  precipitates were obtained by fitting the scattering intensity spectrum. The model used was based on a poly-

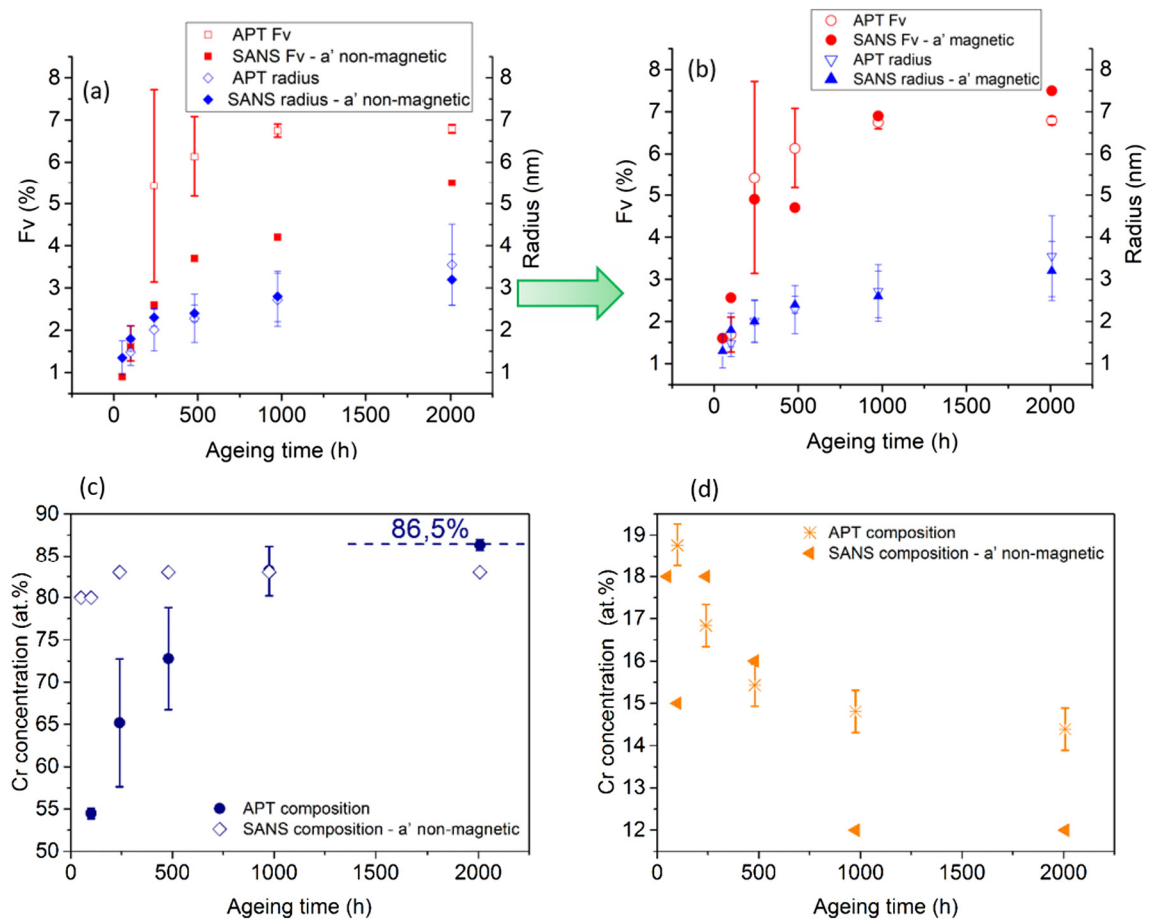


**Fig. 7.** Comparison between mean radius and volume fraction ( $F_v$ ) determined by APT and SANS (a) with the first SANS data treatments and (b) using  $\alpha$  and  $\alpha'$  APT compositions as input data for SANS data fitting. Comparison between (c) precipitates composition and (d) matrix composition determined by both APT and SANS when  $\alpha'$  particles are considered as non-magnetic nano-features. For the second data treatment method, APT compositions were used as input for data treatment.

**Table 1**

Mean radius and volume fraction determined with SANS with the help of APT compositions as data for fits, in the Fe-19 at.%Cr aged from 50 h to 2008 h.

Ageing time (h)	Volume fraction (%)	Mean radius (nm)
50	1,6	1,3 ± 0,4
100	2,56	1,8 ± 0,4
240	4,9	2,0 ± 0,5
480	4,7	2,4 ± 0,2
976	6,9	2,6 ± 0,6
2008	7,5	3,2 ± 0,7

dispersed system with hard spheres interferences. The hard sphere radius is an adjustable parameter which reflects that two precipitates cannot be at a distance from each other, less than twice this radius for various reasons: no interpenetration, existence of a zone of depletion of the matrix around each precipitate. A Gaussian distribution of particles with size  $r$  and standard deviation  $dr$  was assumed, with an estimated volume fraction and contrasts. The adjustments were made on all the intensities (magnetic, nuclear and the sum of the two) to test the coherence of the obtained sets of parameters. Only the adjustments performed on the overall intensities measured in the direction perpendicular to the field gave satisfactory results on all the samples. This is explained by the fact that these intensities are higher and less dependent on the normalization steps (subtraction of the backgrounds...) than the purely nuclear intensity at large angle. Thus, the contrasts were estimated with supposing  $(X\%Cr-(100-X)\%Fe)$   $\alpha'$  particles in a  $(Y\%Fe-(100-Y)\%Cr)$  matrix with  $X$  varying from 80 to 83 and  $Y$  from 18 to

12 depending on the ageing time considered, in order to follow the A ratio variation. The parameters deduced from the best fits of experimental SANS data are plotted in Fig. 7(a, c and d). For all the samples, the hard sphere radius is about 1.5 to 2 times the mean particles radius. That is usually found in equivalent systems.

Unlike APT measurements,  $\alpha'$  particles were detected by SANS after 50 h of ageing. A good agreement between SANS and APT was found for the mean particles radius and size distribution for ageing time longer than 50 h. Nevertheless, the evolution of the volume fraction of precipitates was slower with SANS than with APT. The equilibrium Cr content of the matrix was estimated from the A values to be 12 at.%Cr which was quite low compared to APT data and to values reported in the literature [7,44]. Moreover, regarding the Cr concentration of the matrix with ageing time, there was a drop of the composition down to 15 at.%Cr after 100 h of ageing. This drop was due to adjustment of composition to fit experimental data. But more importantly, conservation of matter was not respected with these adjusted compositions and volume fractions. Bergner et al. [8,10] also fitted A ratio values but considering matter conservation. In their case also, it was not possible to agree with APT data. The treatment of SANS data obtained on a system of which neither the precipitated volume fraction nor the chemical composition of the particles is known is difficult because the mathematical solution is not unique. This approach is made even more complex by the magnetic properties of the FeCr system which are mostly unknown at the particle-matrix interfaces and which can influence the results. It is thus of utmost importance to apply another method of data treatment that will guarantee matter conservation and perhaps obtain good agreement with APT data.

- Second method of SANS data treatments

In order to check whether APT and SANS results can agree, APT compositions were used as input data to fit SANS intensity. The new adjustments have therefore been made under the same conditions as previously, but by calculating the new contrasts with the chemical compositions of the precipitates and of the matrix determined by APT, independently of the A ratio. According to APT measurements (Fig. 3(b)), between 100 h and 480 h, the Cr content of  $\alpha'$  precipitates is lower than roughly 70%, value below which particles should be magnetic. Indeed, following Xiong et al. [40] chart, 70% corresponds to the Curie temperature at 300 K. FeCr alloys which contains < 70% of Cr should be ferromagnetic. This implies that for these ageing times,  $\alpha'$  particles can no longer be considered as non-magnetic scattering features. The magnetic scattering length in the Fe rich particles was calculated in the same way as the matrix's one, using the relation between mean atomic magnetic moment and the Cr content given by Aldred [39]. Fits of scattering intensity spectrum were done with a set of contrast values deduced from this new magnetic hypothesis (for 50 h composition of clusters observed after 100 h was used). It must be emphasized that A ratio of 2.2 was also obtained considering the high proportion of Fe when particles were considered magnetic (see supplemental table). The obtained values of radius and volume fraction are reported in Table 1.

Comparison of these data with APT data is presented in Fig. 7(b). Very interestingly, APT and SANS now agree very well on the volume fraction of  $\alpha'$  particles whereas agreement on mean radius evolution is still excellent. A ratios, which are equal to 2.2, are in good agreement with experimental raw data. And importantly, in this case, matter conservation is respected. APT and SANS agree on composition of particles and matrix (it is normal as there were used as input) and on size and volume fraction of particles. Some question could be raised concerning the particles which contain 70% of Cr because it corresponds to the limit of ferromagnetism/paramagnetism and, this limit was defined for bulk materials not nanoparticles. Measurement of magnetism should allow being more specific on this point. However, these results show that agreement between APT and SANS is possible if  $\alpha'$  particles are considered as magnetic features thanks to Aldred [39] formalism during the early stages of ageing. This last point is also in fact debatable as this formalism was obtained for bulk materials with different composition from those considered here. Indeed, the Cr nanoparticles' magnetism is a very complex issue that was not solved yet.

Anyway, for the first time, SANS and APT agree on all the characteristics of  $\alpha/\alpha'$  precipitation kinetics. And very importantly, these results confirm that Cr evolution of  $\alpha'$  particles with ageing time is a kinetic effect as modelled by Svetukhin et al. [46] and does not originate from an artificial dilution of small precipitates due to local magnification effects.

#### 4. Conclusion

In summary, kinetic of phase separation was investigated using APT and SANS in a Fe-19 at.%Cr alloy aged at 500 °C from 50 h to 2008 h. Two different SANS data treatments were used: the most used method in the literature to treat SANS data where  $\alpha'$  particles are considered as non-magnetic nano-features and a second one where  $\alpha'$  particles are considered as magnetic nano-features at the early stages and non-magnetic as soon as the Cr content of  $\alpha'$  particles exceeds 70%. Results show good agreement between SANS and APT with the second method. For the first time, SANS and APT agree providing that  $\alpha'$  particles are treated as magnetic particles in the early stage of precipitation for SANS data treatment.

#### Acknowledgements

The research was partly supported by the EC project MatISSE (Grant

Agreement No. 604862). The authors acknowledge A. Barbu, F. Soisson and F. Bergner for fruitful discussions and A. Fraczkiwicz for high purity alloy realisation.

#### References

- [1] R.L. Klueh, D.R. Harries, High-chromium Ferritic and Martensitic Steels for Nuclear Application, ASTM, 2001.
- [2] F. Garner, M. Toloczko, B. Sencer, Comparison of swelling and irradiation creep behavior of fcc-austenitic and bcc-ferritic/martensitic alloys at high neutron exposure, *J. Nucl. Mater.* 276 (2000) 123.
- [3] E.A. Little, Development of radiation resistant materials for advanced nuclear power plant, *Mater. Sci. Technol.* 22 (2006) 491–518, <https://doi.org/10.1179/174328406X90998>.
- [4] P. Yvon, F. Carré, Structural materials challenges for advanced reactor systems, *J. Nucl. Mater.* 385 (2009) 217–222, <https://doi.org/10.1016/j.jnucmat.2008.11.026>.
- [5] K.L. Murty, I. Charit, Structural materials for Gen-IV nuclear reactors: challenges and opportunities, *J. Nucl. Mater.* 383 (2008) 189–195, <https://doi.org/10.1016/j.jnucmat.2008.08.044>.
- [6] F. Bley, Neutron small-angle scattering study of unmixing in FeCr alloys, *Acta Metall. Mater.* 40 (1992) 1505–1517.
- [7] S. Novy, P. Pareige, C. Pareige, Atomic scale analysis and phase separation understanding in a thermally aged Fe-20at.%Cr alloy, *J. Nucl. Mater.* 384 (2009) 96–102, <https://doi.org/10.1016/j.jnucmat.2008.10.008>.
- [8] F. Bergner, A. Ulbricht, C. Heintze, Estimation of the solubility limit of Cr in Fe at 300 °C from small-angle neutron scattering in neutron-irradiated Fe-Cr alloys, *Scr. Mater.* 61 (2009) 1060–1063, <https://doi.org/10.1016/j.scriptamat.2009.08.028>.
- [9] V. Kuksenko, C. Pareige, P. Pareige, Cr precipitation in neutron irradiated industrial purity Fe-Cr model alloys, *J. Nucl. Mater.* 432 (2013) 160–165, <https://doi.org/10.1016/j.jnucmat.2012.07.021>.
- [10] F. Bergner, C. Pareige, V. Kuksenko, L. Malerba, P. Pareige, A. Ulbricht, A. Wagner, Critical assessment of Cr-rich precipitates in neutron-irradiated Fe-12at.%Cr: comparison of SANS and APT, *J. Nucl. Mater.* 442 (2013) 463–469, <https://doi.org/10.1016/j.jnucmat.2013.05.023>.
- [11] M. Bachhav, G. Robert Odette, E.A. Marquis,  $\alpha'$  precipitation in neutron-irradiated Fe-Cr alloys, *Scr. Mater.* 74 (2014) 48–51, <https://doi.org/10.1016/j.scriptamat.2013.10.001>.
- [12] O. Tissot, C. Pareige, E. Meslin, B. Decamps, J. Henry, Kinetics of  $\alpha'$  precipitation in an electron-irradiated Fe15Cr alloy, *Scr. Mater.* 122 (2016) 31–35, <https://doi.org/10.1016/j.scriptamat.2016.05.021>.
- [13] E.R. Reese, M. Bachhav, P. Wells, T. Yamamoto, G. Robert Odette, E.A. Marquis, On  $\alpha'$  precipitate composition in thermally annealed and neutron-irradiated Fe-9-18Cr alloys, *J. Nucl. Mater.* 500 (2018) 192–198, <https://doi.org/10.1016/j.jnucmat.2017.12.036>.
- [14] D. Blavette, F. Vurpillot, P. Pareige, A. Menand, A model accounting for spatial overlaps in 3D atom-probe microscopy, *Ultramicroscopy* 89 (2001) 145–153, [https://doi.org/10.1016/S0304-3991\(01\)00120-6](https://doi.org/10.1016/S0304-3991(01)00120-6).
- [15] E.A. Marquis, F. Vurpillot, Chromatic aberrations in the field evaporation behavior of small precipitates, *Microsc. Microanal.* 14 (2008) 561–570, <https://doi.org/10.1017/S1431927608080793>.
- [16] W. Lefebvre-Ulrikson, F. Vurpillot, X. Sauvage, Atom Probe Tomography, Academic Press, <https://www.sciencedirect.com/science/article/pii/B9780128046470010019>, (2016), Accessed date: 2 February 2017.
- [17] J.M. Hyde, G. DaCosta, C. Hatzoglou, H. Weekes, B. Radiguet, P.D. Styman, F. Vurpillot, C. Pareige, A. Etienne, G. Bonny, N. Castin, L. Malerba, P. Pareige, Analysis of radiation damage in light water reactors: comparison of cluster analysis methods for the analysis of atom probe data, *Microsc. Microanal.* (2017) 1–10, <https://doi.org/10.1017/S1431927616012678>.
- [18] C. Hatzoglou, B. Radiguet, P. Pareige, Experimental artefacts occurring during atom probe tomography analysis of oxide nanoparticles in metallic matrix: quantification and correction, *J. Nucl. Mater.* 492 (2017) 279–291, <https://doi.org/10.1016/j.jnucmat.2017.05.008>.
- [19] C. Hatzoglou, B. Radiguet, F. Vurpillot, P. Pareige, A chemical composition correction model for nanoclusters observed by APT - application to ODS steel nanoparticles, *J. Nucl. Mater.* 505 (2018) 240–248, <https://doi.org/10.1016/j.jnucmat.2018.03.057>.
- [20] J.M. Hyde, M.G. Burke, G.D.W. Smith, P. Styman, H. Swan, K. Wilford, Uncertainties and assumptions associated with APT and SANS characterisation of irradiation damage in RPV steels, *J. Nucl. Mater.* 449 (2014) 308–314, <https://doi.org/10.1016/j.jnucmat.2013.07.029>.
- [21] X. Xu, J. Odqvist, M.H. Colliander, M. Thuvander, A. Steuwer, J.E. Westraadt, S. King, P. Hedström, Structural characterization of phase separation in Fe-Cr: a current comparison of experimental methods, *Metall. Mater. Trans. A* 47 (2016) 5942–5952, <https://doi.org/10.1007/s11661-016-3800-4>.
- [22] S.A. Briggs, P.D. Edmondson, K.C. Littrell, Y. Yamamoto, R.H. Howard, C.R. Daily, K.A. Terrani, K. Sridharan, K.G. Field, A combined APT and SANS investigation of  $\alpha'$  phase precipitation in neutron-irradiated model FeCrAl alloys, *Acta Mater.* (2017), <https://doi.org/10.1016/j.actamat.2017.02.077>.
- [23] L. Couturier, F. De Geuser, A. Deschamps, Direct comparison of Fe-Cr unmixing characterization by atom probe tomography and small angle scattering, *Mater. Charact.* 121 (2016) 61–67, <https://doi.org/10.1016/j.matchar.2016.09.028>.
- [24] R.G. Carter, N. Soneda, K. Dohi, J.M. Hyde, C.A. English, W.L. Server, Microstructural characterization of irradiation-induced Cu-enriched clusters in

- reactor pressure vessel steels, *J. Nucl. Mater.* 298 (2001) 211–224, [https://doi.org/10.1016/S0022-3115\(01\)00659-6](https://doi.org/10.1016/S0022-3115(01)00659-6).
- [25] M.K. Miller, B.D. Wirth, G.R. Odette, Precipitation in neutron-irradiated Fe–Cu and Fe–Cu–Mn model alloys: a comparison of APT and SANS data, *Mater. Sci. Eng. A* 353 (2003) 133–139, [https://doi.org/10.1016/S0921-5093\(02\)00679-2](https://doi.org/10.1016/S0921-5093(02)00679-2).
- [26] E. Meslin, M. Lambrecht, M. Hernández-Mayoral, F. Bergner, L. Malerba, P. Pareige, B. Radiguet, A. Barbu, D. Gómez-Briceño, A. Ulbricht, A. Almazouzi, Characterization of neutron-irradiated ferritic model alloys and a RPV steel from combined APT, SANS, TEM and PAS analyses, *J. Nucl. Mater.* 406 (2010) 73–83, <https://doi.org/10.1016/j.jnucmat.2009.12.021>.
- [27] F. Vurpillot, A. Bostel, D. Blavette, Trajectory overlaps and local magnification in three-dimensional atom probe, *Appl. Phys. Lett.* 76 (2000) 3127–3129, <https://doi.org/10.1063/1.126545>.
- [28] T.T. Tsong, Field ion image formation, *Surf. Sci.* 70 (1978) 211–233.
- [29] V. Kuksenko, C. Pareige, C. Genevois, F. Cuvilly, M. Roussel, P. Pareige, Effect of neutron-irradiation on the microstructure of a Fe–12at.%Cr alloy, *J. Nucl. Mater.* 415 (2011) 61–66, <https://doi.org/10.1016/j.jnucmat.2011.05.042>.
- [30] C. Pareige, V. Kuksenko, P. Pareige, Behaviour of P, Si, Ni impurities and Cr in self ion irradiated Fe–Cr alloys – comparison to neutron irradiation, *J. Nucl. Mater.* 456 (2015) 471–476, <https://doi.org/10.1016/j.jnucmat.2014.10.024>.
- [31] E. Meslin, B. Radiguet, M. Loyer-Prost, Radiation-induced precipitation in a ferritic model alloy: an experimental and theoretical study, *Acta Mater.* 61 (2013) 6246–6254, <https://doi.org/10.1016/j.actamat.2013.07.008>.
- [32] D.J. Larson, T.J. Prosa, R.M. Ulfig, B.P. Geiser, T.F. Kelly, Local Electrode Atom Probe Tomography, Springer New York, New York, NY, 2013 <http://link.springer.com/10.1007/978-1-4614-8721-0> (accessed April 26, 2016).
- [33] M.P. Moody, J.M. Cairney, B. Gault, S.P. Ringer, *Atom Probe Microscopy*, vol. 160, Springer Series in Materials Science, 2012, <http://www.springer.com/materials/characterization+%26+evaluation/book/978-1-4614-3435-1>, Accessed date: 24 October 2012.
- [34] M. Miller, A. Cerezo, M. Hetherington, G. Smith, *Atom Probe Field Ion Microscopy*, Clarendon, Oxford, 1996.
- [35] M. Miller, *Atom Probe Tomography*, Kluwer Academic/Plenum Publishers, New York, 2000.
- [36] J.P. Cotton, Article, *J. Phys. IV* 9 (1999), <https://doi.org/10.1051/jp4:1999103Pr1-21>.
- [37] M.S. Wertheim, Exact solution of the Percus-Yevick integral equation for hard spheres, *Phys. Rev. Lett.* 10 (1963) 321–323, <https://doi.org/10.1103/PhysRevLett.10.321>.
- [38] E. Thiele, Equation of state for hard spheres, *J. Chem. Phys.* 39 (1963) 474–479, <https://doi.org/10.1063/1.1734272>.
- [39] A.T. Aldred, Ferromagnetism in iron-chromium alloys. I. Bulk magnetization measurements, *Phys. Rev. B* 14 (1976) 219–227, <https://doi.org/10.1103/PhysRevB.14.219>.
- [40] W. Xiong, M. Selleby, Q. Chen, J. Odqvist, Y. Du, Phase equilibria and thermodynamic properties in the Fe–Cr system, *Crit. Rev. Solid State Mater. Sci.* 35 (2010) 125–152, <https://doi.org/10.1080/10408431003788472>.
- [41] M. Mathon, Y. de Carlan, G. Geoffroy, X. Averty, A. Alamo, C. de Novion, A SANS investigation of the irradiation-enhanced  $\alpha$ - $\alpha'$  phases separation in 7–12 Cr martensitic steels, *J. Nucl. Mater.* 312 (2003) 236–248, [https://doi.org/10.1016/S0022-3115\(02\)01630-6](https://doi.org/10.1016/S0022-3115(02)01630-6).
- [42] G. Porod, Small angle x-ray scattering. Von O. GLATTER und O. KRATKY. London: Academic Press Inc. Ltd. 1982. ISBN 0-12-286280-5. X, 515 Seiten, geb. £ 43,60; US \$ 81.00. *Acta Polym.* 36 (1985) 296, <https://doi.org/10.1002/actp.1985.010360520>.
- [43] M. Thuvander, H.-O. Andrén, K. Stiller, Q.-H. Hu, A statistical method to detect ordering and phase separation by APFIM, *Ultramicroscopy* 73 (1998) 279–285, [https://doi.org/10.1016/S0304-3991\(97\)00168-X](https://doi.org/10.1016/S0304-3991(97)00168-X).
- [44] S.M. Dubiel, G. Inden, On the miscibility gap in the Fe–Cr system: a mössbauer study on long term annealed alloys, *Z. Metallkd.* 78 (1987) 544–549.
- [45] W.-Y. Chen, Y. Miao, Y. Wu, C.A. Tomchik, K. Mo, J. Gan, M.A. Okuniewski, S.A. Maloy, J.F. Stubbins, Atom probe study of irradiation-enhanced  $\alpha'$  precipitation in neutron-irradiated Fe–Cr model alloys, *J. Nucl. Mater.* 462 (2015) 242–249, <https://doi.org/10.1016/j.jnucmat.2015.04.005>.
- [46] V. Svetukhin, P. L'vov, E. Gaganidze, M. Tikhonchev, C. Dethloff, Kinetics and thermodynamics of Cr nanocluster formation in Fe–Cr system, *J. Nucl. Mater.* 415 (2011) 205–209, <https://doi.org/10.1016/j.jnucmat.2011.06.005>.
- [47] J. Cahn, J. Hilliard, Free energy of a nonuniform system. 3. Nucleation in a 2-component incompressible fluid, *J. Chem. Phys.* 31 (1959) 688–699, <https://doi.org/10.1063/1.1730447>.
- [48] C. Zhang, M. Enomoto, Study of the influence of alloying elements on Cu precipitation in steel by non-classical nucleation theory, *Acta Mater.* 54 (2006) 4183–4191, <https://doi.org/10.1016/j.actamat.2006.05.006>.